First-principles investigation of phase stability in Li_xCoO_2

A. Van der Ven, M. K. Aydinol, and G. Ceder
Department of Materials Science and Engineering, Massachusetts Institute of Technology, 77 Massachusetts Avenue, Cambridge, Massachusetts 02139

G. Kresse and J. Hafner
Institut fur Theoretische Physik, Technische Universität Wien, Wiedner Hauptstrasse 8-10/136, A-1040 Wien, Austria
(Received 6 February 1998)

In this work, the phase diagram of Li_xCoO_2 is calculated from first principles for x ranging from 0 to 1. Our calculations indicate that there is a tendency for Li ordering at $x=\frac{1}{2}$ in agreement with experiment [J. N. Reimers and J. R. Dahn, J. Electrochem. Soc. **139**, 2091 (1992)]. At low Li concentration, we find that a staged compound is stable in which the Li ions selectively segregate to every other Li plane leaving the remaining Li planes vacant. We do not find the two-phase region observed at high Li concentration and speculate that this two-phase region is caused by the metal-insulator transition that occurs at concentrations slightly below $x=1$. [S0163-1829(98)06529-1]

I. INTRODUCTION

Li_xCoO_2 has served as an archetypal cathode material for secondary Li batteries ever since the discovery by Mizushima *et al.*[1] that Li can be reversibly removed from and reinserted into Li_xCoO_2. The layered form of $LiCoO_2$, which has rhombohedral symmetry and belongs to the space group $R\bar{3}m$, is ideally suited to accommodate large changes in Li concentration. This crystal structure consists of close-packed oxygen layers stacked in an ABC sequence with Co and Li ions residing in octahedral sites in alternating layers between the oxygen planes.[2] Figure 1 illustrates the crystal structure of the layered form of $LiCoO_2$. As the Li concentration is changed in Li_xCoO_2, vacancies are created or annihilated within the Li planes.

Li_xCoO_2 exhibits many of the essential properties required of a reliable cathode material. The voltage of Li_xCoO_2 with respect to metallic lithium is sufficiently high to guarantee a high-energy density though not too high to cause electrolyte breakdown. Furthermore, Li_xCoO_2 undergoes only small structural changes as it is deintercalated to a Li concentration of approximately 0.3. When the variations in Li concentration are limited between $x=0.5$ and 1.0, the intercalation reaction is perfectly reversible giving rise to batteries with exemplary cyclability.

In addition to its favorable electrochemical properties, Li_xCoO_2 also exhibits a variety of phase transformations that are typical of many intercalation compounds. Reimers and Dahn,[3] for example, observed that the Li ions order in rows at $\frac{1}{2}$ Li concentration. They carefully measured the stability region of this ordered phase and determined its order-disorder transition temperature to be about 60 °C. Another transformation of an electronic nature occurs at high Li concentration. $LiCoO_2$ is a semiconductor[4] while Li_xCoO_2 at concentrations below $x=0.75$ is metallic,[5] implying that a metal-insulator transition occurs at intermediate Li concentration. Curiously, superimposed on this metal-insulator transition is a two-phase coexistence region between crystallographically identical host structures. At room temperature, this two-phase coexistence region is found to exist between the Li concentrations of $x=0.75$ and 0.93.[1,6] At dilute Li concentrations, transformations of yet another type occur, involving structural changes of the layered host. As the Li concentration is brought below about $x=0.21$, the layered crystal structure of Fig. 1 is observed to undergo a phase transformation in which the lattice parameters change significantly.[6,7] The phase to which the host transforms has not been identified. Recently, Amatucci, Tarascon, and Klein[7] have shown that Li_xCoO_2 can be completely and re-

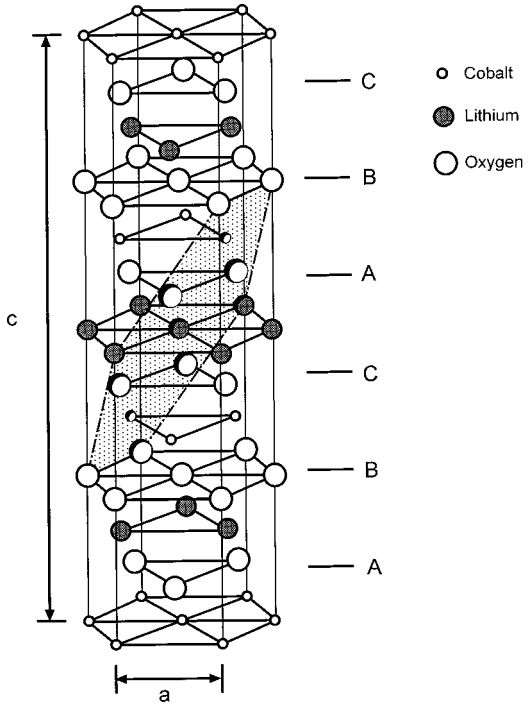

FIG. 1. The crystal structure of the layered form of $LiCoO_2$. The oxygen ions form close-packed planes stacked in an $ABCABC$ sequence, and the cobalt and lithium ions occupy alternating layers of octahedral sites. The shaded plane will be referred to in Fig. 5.

 © 1998 The American Physical Society

versibly deintercalated to form CoO_2. They found that in the CoO_2 phase, the different O-Co-O slabs, held together by van der Waals forces, are shuffled with respect to each other, such that the close-packed oxygen layers have an *ABAB* stacking sequence as opposed to the *ABCABC* sequence of $LiCoO_2$.[7]

The spectrum of phase-transformation phenomena in Li_xCoO_2 makes this material ideally suited for a fundamental study of the nature and thermodynamic driving forces of phase transformations in transition-metal-oxide intercalation compounds. For applications in a rechargeable battery, phase transformations as a function of Li concentration are undesirable as they are often accompanied by irreversibilities and large volume changes. An understanding of the origins of these phase transformations can therefore be valuable in the design of new cathode materials. First-principles investigations are proving to be an invaluable tool in this respect.[8–17]

Phase stability is best represented in a phase diagram that maps the thermodynamically stable phases as a function of temperature and Li concentration. The main ingredient in the construction of a phase diagram is the free energy of the phases competing for stability. Much progress has been made over the past 15 years in the first-principles calculation of free energies and prediction of ordering in systems with substitutional degrees of freedom. Typically, such calculations involve a combination of accurate first-principles total-energy calculations and statistical-mechanics techniques (e.g., the cluster variation method or Monte Carlo techniques) to obtain finite-temperature thermodynamic properties. The bridge between total-energy calculations and statistical-mechanics techniques lies in the cluster expansion formalism that enables an accurate and rapid extrapolation of the total energy of any configuration from the first-principles energy values of a relatively small number of configurations.[9,16,18]

In this paper, we investigate the phase diagram of the layered form of Li_xCoO_2 from first principles. In Sec. II, the cluster expansion formalism and its application to first-principles calculations is described. In Sec. III, we present the results of our investigation of the Li_xCoO_2 system. In this section, we first describe three different host structures whose relative stability we investigated as a function of Li concentration and temperature (Sec. III A). In Sec. III B and III C, we present the results of our *ab initio* pseudopotential calculations for different Li vacancy arrangements within Li_xCoO_2. These results were used to construct cluster expansions to describe the configurational energy of different Li-vacancy arrangements (Sec. III D). In Sec. IV, the calculated Li_xCoO_2 phase diagram is presented. This section is followed by a discussion of the results.

II. METHOD

The determination of the relative stability of different phases at finite temperature must be done by a comparison of their free energies. Statistical mechanics tells us how a macroscopic thermodynamic property such as the free energy can be determined from the detailed microscopic interactions between the atoms of a solid. The link lies in the partition function Z of the solid, which is defined as

$$Z=\sum_s \exp\left(\frac{-E_s}{k_BT}\right), \tag{1}$$

where k_B is the Boltzmann constant, T is the absolute temperature, and E_s is the energy of a state s in which the solid can reside. The summation in Eq. (1) extends over all possible states s corresponding to different configurational states (e.g., different Li and vacancy arrangements), vibrational states, electronic states, etc. The free energy is related to the partition function according to

$$F=-k_BT\,\ln(Z). \tag{2}$$

In most first-principles investigations of solids with configurational degrees of freedom,[9,11,16,19,20] the effect of vibrational and electronic excitations are neglected. The inclusion of these degrees of freedom generally leads to only quantitative improvements in order-disorder transition temperatures.[21] In this work, we neglect the electronic and vibrational degrees of freedom and consider only the contributions to the free energy of the configurational degrees of freedom associated with Li and vacancy distributions within different CoO_2 hosts. The sum in Eq. (1) is then over the different configurational states only.

In systems with configurational degrees of freedom, it is convenient to describe properties that depend on configuration, such as the configurational energy, with a *cluster expansion*.[8,9,11,22] To construct a cluster expansion for Li configurations within a particular CoO_2 host, we assign an occupation variable σ_i to each possible Li site i, which takes the value $+1$ if Li resides at that site and -1 if a vacancy is at that site. It has been shown that the dependence of any property on configuration can be exactly expanded in terms of polynomials φ_α of these discrete occupation variables σ_i.[22] φ_α is defined as a product of occupation variables $\sigma_i,\sigma_j,\ldots,\sigma_k$, where the indices $i,j,\ldots,k$ correspond to a collection of sites that form a cluster α, such as a pair cluster, a triplet cluster, etc. A cluster expansion of the energy, for example, takes the form

$$E=V_0+\sum_\alpha V_\alpha\varphi_\alpha, \tag{3}$$

where the sum in Eq. (3) extends over all possible clusters of sites α. V_0 and the coefficients V_α are called effective cluster interactions (ECI) and have a constant value. The ECI are merely expansion coefficients describing the dependence of the energy of the crystal on the Li-vacancy configurations and are not to be confused with interaction potentials commonly used in oxides. In practice, the ECI (V_α) converge to zero as the size or distance between the points of the cluster α increase. Equation (3) can therefore be truncated after some maximal cluster. It is important to note that the Li ions do not have to reside exactly at the lattice sites i in order for a cluster expansion to be applicable. Relaxations are allowed within the cluster expansion formalism and both relaxations of the Li ions and of the CoO_2 host are implicitly accounted for in the numerical values of the ECI. All that is required for a cluster expansion to be applicable is that there exists a one-to-one correspondence between the relaxed Li ions and the sites i to which an occupation variable σ_i is assigned.

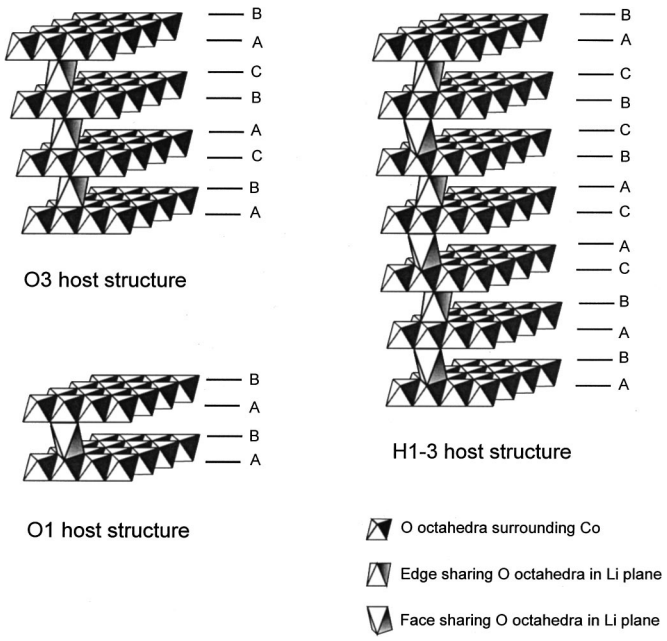

FIG. 2. Schematic illustration of the three host structures O3, O1, and *H*1-3. The vertices of the octahedra correspond to oxygen ions. The uppercase letters describe the stacking sequence of the close-packed oxygen layers in each host. Depending on the host structure, the oxygen octahedra surrounding the Li sites share edges with the oxygen ions surrounding the Co ions (i.e., the O3 host) or they share faces (i.e., the O1 host). In the *H*1-3 host, oxygen octahedra around the Li sites of every other plane between O-Co-O slabs share edges with the octahedra surrounding Co ions as in O3 while in the remaining planes these octahedra share faces as in O1.

The values of the ECI for a particular system must be determined with an accurate first-principles method. Typically this occurs by calculating the energy of a series of configurations (e.g., different Li-vacancy arrangements within a particular host) using a first-principles method and then fitting a truncated form of Eq. (3) to the values of these energies. The fit to the first-principles energies can be performed with either a least-squares procedure[23] or a more elaborate method based on linear programming techniques.[24] Once an accurate cluster expansion has been constructed, the total energy of any Li-vacancy arrangement can be calculated rapidly. This makes it possible to calculate finite-temperature thermodynamic properties using statistical-mechanics techniques such as Monte Carlo simulations.[25]

III. RESULTS

A. Host structures

To investigate phase stability with the cluster expansion method, we must consider the set of host structures that are likely to be stable as a function of Li concentration and temperature. In this work, we considered three host structures. These are illustrated in Fig. 2. In this figure, the vertices of the octahedra schematically represent the oxygen sites that coordinate the Co ions at the center of these octahedra. The Li ions reside in octahedral sites between the O-Co-O slabs. For each host, a representative oxygen octahedra surrounding a Li site is drawn in Fig. 2. The first host structure is the layered form of $LiCoO_2$, conventionally called O3,[26] which has an ABC oxygen stacking. This structure is observed to be stable experimentally for Li concentrations between $x = 0.3$ and 1.0.[3,6,7] This is the same structure as illustrated in Fig. 1. The second host in Fig. 2, referred to as O1, has an *ABAB* oxygen stacking. This structure is observed to be more stable than the O3 host when Li_xCoO_2 is completely deintercalated[7] (i.e., $x=0$). First-principles calculations with the linearized augmented plane wave method (LAPW) have supported this experimental finding[27] by predicting that CoO_2 in the O1 structure has a lower energy than O3 by about 50 meV per $\varnothing CoO_2$ formula unit, where $\varnothing$ represents a Li vacancy.[27] The stability of the O1 host seems to be restricted only to zero Li concentration. Both experimental and first-principles evidence suggest that the O1 host is unstable when Li is inserted in CoO_2: Amatucci, Tarascon, and Klein[7] observed that the O1 host immediately reverts back to the O3 host upon Li intercalation into CoO_2. Furthermore, LAPW calculations have shown that the O1 form of $LiCoO_2$ is less stable than O3 by 150 meV per formula unit.[27] This indicates that the Li ions prefer the octahedral sites of O3 to those of O1. The reason for this preference can be attributed to a lower electrostatic energy of Li in O3 as compared to that of Li in O1. In the O3 host, the oxygen octahedra surrounding Li sites share edges with the octahedra surrounding the Co sites, whereas in the O1 host, they share faces. The electrostatic repulsion between the Li and Co ions is greater in the latter case.

The third host structure that we considered has features of both O3 and O1. In this hybrid host, which we will refer to as *H*1-3, every other plane between O-Co-O slabs has an environment identical to that of O3 whereas the remaining planes have an environment identical to that of O1. Since as described above, Li prefers the octahedral sites of O3 to those of O1, we assumed that in *H*1-3, the Li ions only occupy those alternating planes with an O3 environment. In view of this assumed distribution of Li ions between the O-Co-O slabs, this hybrid host structure can be thought of as a stage-II compound similar to that observed in graphite intercalation compounds.[28] Since Li intercalates only into every other plane between O-Co-O slabs of *H*1-3, the maximum Li concentration that can be obtained in this host is $x = \frac{1}{2}$ in Li_xCoO_2. The crystallographic details and the x-ray powder-diffraction patterns of this phase have been published elsewhere.[29] Similarly to O3, *H*1-3 at the stoichiometries CoO_2 and $Li_{1/2}CoO_2$ also belongs to the $R\bar{3}m$ space group. The unit cell of *H*1-3 in the hexagonal setting has the same **a** lattice vector as O3; however, it has a **c** lattice vector that is twice as large as that of O3.

In all hosts, we assumed that the Co ions do not migrate to the Li planes when Li vacancies are introduced there. Unlike for the layered form of Li_xNiO_2 Ref. 30 there is to our knowledge no experimental evidence suggesting that Co ions leave the Co planes to reside in vacant Li sites. Furthermore, a first-principles investigation of Co and Li ordering in $LiCoO_2$ and of Co and vacancy ordering in CoO_2 Refs. 27 and 31 indicated that there is no thermodynamic driving force for intermixing of Co and Li. In this work, we investigate the energetics and thermodynamics resulting from the

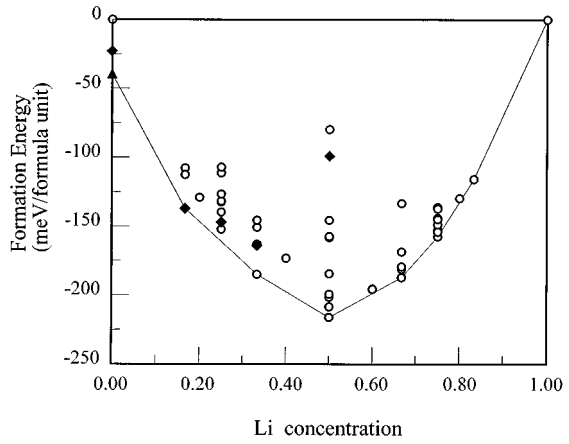

FIG. 3. The formation energies as calculated with the pseudopotential method of (i) 44 different Li-vacancy arrangements within the O3 host (open circles), (ii) five different Li-vacancy arrangements within the $H1$-3 (filled diamonds), and (iii) CoO_2 in the O1 host (filled triangle).

degrees of freedom associated with Li-vacancy rearrangement over the octahedral sites in the Li planes of the O3 and $H1$-3 hosts.

The three host structures O3, O1, and $H1$-3 are very similar to each other in that the O-Co-O slabs consist of edge-sharing CoO_6 octahedra. The only difference between them is in the way in which the O-Co-O slabs are related to each other across the Li planes. Each of these host structures can be derived from the other by a simple gliding of the O-Co-O slabs with respect to each other adjacent to an empty Li plane. For example, the O3 host can be transformed to the $H1$-3 host by gliding the O-Co-O slabs adjacent to every other Li plane, whereas O1 can be obtained from O3 by gliding the O-Co-O slabs adjacent to every Li plane. These types of glides are likely to have small activation barriers when the Li planes are empty. This means that, if there is a thermodynamic driving force, these glide transformations will likely occur at ambient temperatures. Along with the O3 and O1 hosts that are observed experimentally, the $H1$-3 host is therefore a reasonable candidate structure that can be expected during a typical deintercalation and intercalation cycle at room temperature.

B. Formation energies

The construction of a cluster expansion that reflects the configurational energy of a system requires accurate first-principles total-energy calculations as input. In this work, we used the VIENNA *ab initio* simulation package (VASP) to perform first-principles total-energy calculations for Li_xCoO_2.[32,33] VASP numerically solves the Kohn-Sham equations within the local-density approximation using ultrasoft pseudopotentials[34,35] and a plane-wave basis set. Details of the VASP pseudopotential code can be found in Refs. 32 and 33.

We calculated the total energy of (i) 44 different Li-vacancy arrangements in the O3 host for concentrations ranging from $x=0$ to 1, including CoO_2 and $LiCoO_2$, (ii) five different Li-vacancy arrangements in the $H1$-3 host for concentrations ranging from $x=0$ to $\frac{1}{2}$, and (iii) CoO_2 in the O1 host. The formation energies of the different Li-vacancy configurations are plotted in Fig. 3. We define the formation energy for a given Li-vacancy arrangement with composition x in Li_xCoO_2 as

$$\Delta_f E = E - xE_{LiCoO_2} - (1-x)E_{CoO_2}, \tag{4}$$

where E is the total energy of the configuration per $Li_x\varnothing_{1-x}CoO_2$ formula unit, E_{LiCoO_2} is the energy of $LiCoO_2$ in the O3 host, and E_{CoO_2} is the energy of CoO_2 in the O3 host. We consider formation energy as opposed to total energy because it is the relevant quantity for the study of phase stability. The formation energy of a given structure Li_xCoO_2 as defined in Eq. (4) reflects the relative stability of that structure with respect to phase separation into a fraction x of $LiCoO_2$ and a fraction $(1-x)$ of CoO_2.

To calculate the total energies, we used ultrasoft pseudopotentials[34,35] which allow for a moderately low-energy cutoff for the plane wave basis set expansion. For oxygen, we used a pseudopotential with a core radius of 1.55 a.u. while for Li and Co we used the core radii of 2.6 and 2.46, respectively. Partial core corrections[41] were implemented to treat the nonlinear dependence of the exchange correlation functional.

In all the total-energy calculations, a plane-wave basis set cutoff energy of 600 eV was used. This value was found to be more than sufficient to ensure a converged plane-wave basis set. The exchange and correlation functional implemented in the calculations was that of Ceperley and Alder[36] as parametrized by Perdew and Zunger.[37] k-space sampling was performed with the method of Monkhorst and Pack.[38] The ionic positions and the lattice parameters of each structure were relaxed with the conjugate gradient method using forces and stresses. During relaxation, partial occupancy at the Fermi level was treated with the method of Methfessel and Paxton.[39] After relaxation was achieved, the energies of the optimized geometries were recalculated, this time performing k-space integrations using the linear tetrahedron method including corrections according to Blöchl, Jepsen, and Andersen.[40] Convergence tests of the energy with respect to the k-space grid were performed for several Li-vacancy configurations in the O3 host with supercells that are representative for the remaining Li-$\varnothing$ configurations considered in this work. We found that for the k-point grids used in these supercells, the total energies were converged to within 5 meV per formula unit of $Li_x\varnothing_{1-x}CoO_2$. To determine whether spin polarization is important in Li_xCoO_2, we performed spin-polarized calculations for several Li-vacancy configurations within the O3 host. We found that spin polarization does not affect the total energy of $LiCoO_2$ and lowers the energy of CoO_2 in the O3 host by only 11 meV per formula unit. We determined that the effect of spin polarization on the formation energies is negligible, producing a change of at most 3 meV per $Li_x\varnothing_{1-x}CoO_2$ formula unit. All total-energy calculations used in this work are therefore nonmagnetic.

The formation energies of all structures in Fig. 3 are negative, indicating that Li_xCoO_2 is stable with respect to phase separation into a fraction x of $LiCoO_2$ and a fraction (1

$-x$) of CoO_2 within the O3 host. This means that for sufficiently low temperatures, we can expect that at a particular Li concentration x, the stable phase will either be a stoichiometric compound in which Li and vacancies are ordered on a superlattice, or a mixture of ordered stoichiometric compounds. At higher temperature, these ordered compounds are expected to transform to the disordered state, assuming that the host on which the Li ions order is still stable with respect to other host structures. In Fig. 3, we have drawn the convex hull connecting the structures with the lowest formation energies to indicate which of the structures are the most stable among the those whose energies were calculated with the pseudopotential method.

Several important features about Li_xCoO_2 can be deduced from the formation energies as calculated with the pseudopotential method. Figure 3 shows, in agreement with experiment,[7] that at zero Li concentration the O1 host is more stable than the O3 host. The difference in energy between O1 and O3 is 40 meV per $Li_x\varnothing_{1-x}CoO_2$ formula unit. This result is in good agreement with previous first-principles calculations using the LAPW method which found a value of 50 meV.[27] Approximately halfway between the formation energies of O1 and O3 lies the formation energy of the $H1$-3 host at $x=0$. This is a plausible result since every other empty plane between O-Co-O slabs in the $H1$-3 host has an O3 environment, while the remaining empty planes have an O1 environment. It implies that the interaction between adjacent O-Co-O slabs is fairly short ranged and that the energy of $H1$-3 at $x=0$ could be approximated as the weighted average of the energies of O1 and O3. In addition, the calculated equilibrium c-lattice parameter of $H1$-3 (converted to the setting of the O3 host) is 12.23 Å, which is roughly the average of the calculated c-lattice parameter of O3 of 12.39 Å and that of O1 (also converted to the setting of the O3 host) of 11.99 Å. In Fig. 3 it can be seen that at $x=0.1666$, the Li-vacancy arrangement in the $H1$-3 host lies on the convex hull. This structure is more stable than the two other Li-vacancy arrangements considered on the O3 host at that concentration. Furthermore, the fact that it lies on the convex hull means that it is more stable than a two-phase mixture (with overall Li concentration $x=0.1666$) of any two other ordered Li-vacancy arrangements. As will be shown in the next sections, this result indicates that the $H1$-3 host will appear as a stable phase in the phase diagram. Figure 3 also clearly indicates that there is a tendency for Li ordering within the O3 host at $x=\frac{1}{2}$.

Among the 44 different Li-vacancy configurations considered, the lowest-energy configuration at $x=\frac{1}{2}$ has an in-plane Li ordering as illustrated in Fig. 4(a). In this configuration, the Li ions are ordered in rows separated by rows of vacancies. This in-plane Li ordering is the same as that proposed by Reimers and Dahn[3] based on their electrochemical and *in situ* x-ray powder-diffraction measurements. They deduced this type of Li ordering by noticing that the (104) peak of the O3 host (which has rhombohedral symmetry) splits into two peaks with an intensity ratio of 1:2. Reimers and Dahn[3] argued that this splitting can be explained by assuming that the host changes from a rhombohedral to a monoclinic symmetry whereby the basal plane of the monoclinic structure (containing the a and b lattice vectors) is a two-dimensional supercell of the basal plane of the rhombohedral O3 host in the hexagonal setting. This is illustrated in Fig. 4(a). This still leaves several crystallographically distinct ways to stack in-plane Li-vacancy arrangements along the c direction. Figure 4 also indicates which stacking results in the lowest energy. This is illustrated by projecting the Li-vacancy ordering in two adjacent Li planes along a direction perpendicular to the Li planes.

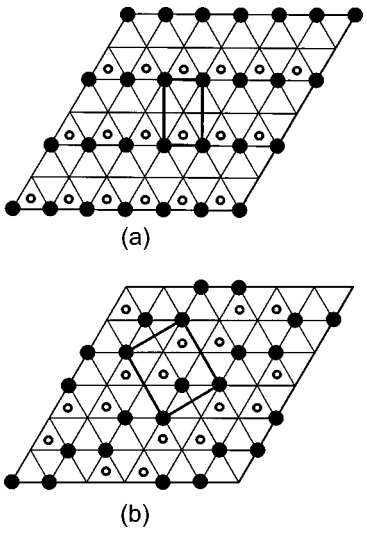

FIG. 4. Two Li-vacancy arrangements at concentration $x=\frac{1}{2}$ in Li_xCoO_2 whose formation energies are very low. The triangular lattice denotes the Li sites within a Li plane of the O3 host. The filled circles correspond to Li ions ordered on the triangular lattice. A given in-plane ordered arrangement of Li ions can be stacked in different ways among the different Li planes. The unfilled circles designate the projection perpendicular to the Li plane of the positions of the Li ions in the adjacent Li plane.

Almost degenerate, but slightly higher in energy with the Li-vacancy ordering of Fig. 4(a) is another structure with the arrangement as illustrated in Fig. 4(b). In this configuration, the Li ions are ordered in a zigzag arrangement. The pseudopotential calculations predict that the formation energy of this structure is approximately 1 meV per $Li_x\varnothing_{1-x}CoO_2$ formula unit higher than that of Fig. 4(a). This difference in energy is too small to be resolved with currently available numerical methods. Therefore, we cannot unequivocally deduce from our first-principles calculations which of the two Li-vacancy configurations is the ground state. We calculated the x-ray powder-diffraction patterns of the fully relaxed coordinates of the structures with the Li-vacancy configurations depicted in Figs. 4(a) and 4(b). The powder-diffraction pattern of the configuration of Fig. 4(a) exhibits the (104) peak splitting observed experimentally.[3] The diffraction pattern of the configuration of Fig. 4(b) does not exhibit this peak splitting. This suggests that the structure of Fig. 4(a) is indeed the stable state at $x=\frac{1}{2}$.

C. Charge transfer and screening

One salient feature about the formation energies in Fig. 3 is that they do not vary strongly with different Li-vacancy configurations at each Li concentration. Previous pseudopotential calculations[13,14] have shown that Li in $LiCoO_2$ is completely ionized. The Li^+ ions are therefore expected to strongly interact electrostatically. Generally, the variation of

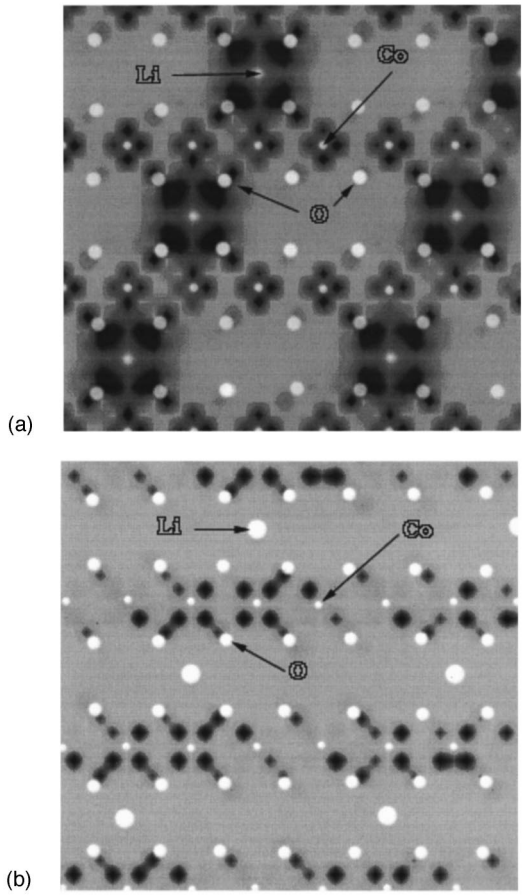

FIG. 5. (a) The positive part of the difference between the electronic density of $Li_{1/4}CoO_2$ and CoO_2 in the O3 host. Dark regions designate regions of high electron density. The large white circles designate the oxygen sites while the small white circles designate the cobalt sites (the circles designating these sites have been superimposed on the charge difference plot). The lithium ions reside at the center of the sets of four oxygen ions with increased electron density. (b) The negative part of the electronic density difference between $Li_{1/4}CoO_2$ and CoO_2 in the O3 host. Dark areas signify regions of electron density depletion. The very large white circles correspond to occupied Li, the intermediate size circles correspond to oxygen sites, and the small circles correspond to Co sites. The crystallographic plane in these figures correspond to the shaded plane illustrated in Fig. 1.

the energy with configuration is large in systems in which the substitutional components are ionized.[16,42] This does not occur in Li_xCoO_2 because the Li ions are strongly screened by the local oxygen environment. Contrary to what is often assumed, previous first-principles calculations[13,14] have indicated that a large fraction of the electron donated by the Li ion to the CoO_2 host is not transferred to Co (thus changing the valence of Co from Co^{4+} to Co^{3+} according to a conventional chemistry point of view) but is transferred to oxygen. By integrating the charge within spheres around the oxygen ions, it was found[13,14] that about 50% of the valence charge from Li is transferred to oxygen. This transferred charge to the oxygen ions effectively screens the strong electrostatic interaction expected between positively charged Li ions.

The effect of Li intercalation on the electron density can be seen in a plot of the difference of the electron densities before and after Li addition. Figure 5 shows a charge difference plot between Li_xCoO_2 at $x=0.25$ and CoO_2 both in the O3 host. For the purpose of this calculation, the lattice parameters and the positions of O and Co were taken to be the same in the two structures such that the charge densities could be subtracted point by point. The resulting difference shows how the electron distribution changes when Li is added to the host, and in particular where the electron of the added Li resides within the host. Figure 5(a) shows the positive part of the charge difference, and therefore indicates the regions in which there is an accumulation of charge upon addition of Li. Figure 5(b) shows the negative part of the charge difference, showing regions in which the electron density is depleted as a result of Li addition. Note that since $x=0.25$ in Li_xCoO_2, only $\frac{1}{4}$ of the Li sites are occupied. The crystallographic plane shown in Fig. 5 corresponds to the shaded plane illustrated in Fig. 1. This plane cuts through Li, Co, and O ions.

Figure 5 clearly shows that although the Li ions are ionized, the electron transfer from Li to the host is very local. There is a significant increase in the electron density at the oxygen sites immediately surrounding the Li ions. The accumulation of electron density at these oxygen sites has a distribution that resembles that of polarized atomic p orbitals. From Fig. 5, it is clear that the local charge transfer from Li to its neighboring oxygen ions forms an almost spherical electron cloud that locally screens the positive charge of the ionized Li ion. This local charge transfer from Li to the neighboring oxygen ions is representative of that occurring in the other structures investigated with the pseudopotential method and explains why the energy does not vary strongly as the Li-vacancy arrangement is changed at fixed Li concentration.

Figures 5(a) and 5(b) illustrate that there is a significant redistribution of charge around the Co ions as Li is added to the host. Figure 5(a) shows that there is an accumulation of charge density in lobes pointing in directions between the oxygen ions. This increase in charge on Co is the result of the electron addition to the t_{2g} bands as Li is added to the host [within the local-density approximation, these bands are partially filled in CoO_2 (Ref. 13)]. The t_{2g} bands in transition-metal oxides in which the transition metal resides in an octahedral environment result from the d_{xy}, d_{xz}, and d_{yz} atomic orbitals of the transition metal that point away from the oxygen ions. Figure 5(b) shows that there is also a significant depletion in electron density around the Co ions closest to the Li ions. This depletion results from a change in the polarization of the σ bonds between the oxygen ions and Co. In an octahedral oxygen environment, the d_{z^2} and $d_{x^2-y^2}$ atomic orbitals of Co directly overlap with the p_x, p_y, and p_z orbitals of oxygen, thus forming bonding e_g^b bands and antibonding e_g^* bands (the e_g^* bands are commonly referred to as simply the e_g bands and lie above the t_{2g} bands in Li_xCoO_2). For strongly ionic crystals, the e_g^* band is primarily of metal d character, while the e_g^b is composed mainly of oxygen p states. The charge depletion in Fig. 5(b) occurs in regions that resemble the charge distribution of a $d_{x^2-y^2}$ atomic orbital (i.e., lobes pointing toward the oxygen ions). Within the local-density approximation, the e_g^* bands of Li_xCoO_2 are empty for all x, and hence this charge depletion

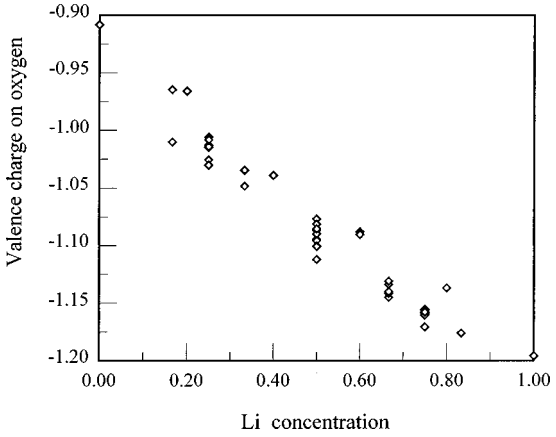

FIG. 6. Integrated valence charge of the oxygen ions in the 44 structures within the O3 host with different Li-vacancy arrangements. This charge is the excess charge on oxygen with respect to the neutral oxygen ion.

implies that a change in the nature of the e_g^b bond between Co and O is occurring. It indicates that as Li is added, this bond becomes more polarized with more electron density accumulating at the oxygen ion. In effect, Li addition to CoO_2 makes the host more ionic in nature.

In Fig. 6, we plot as a function of Li concentration the average net charge on the oxygen ions for the 44 structures having different Li-vacancy arrangements within the O3 host. As can be seen from Fig. 6, the average net charge on oxygen increases almost linearly with Li concentration from a value of -0.9 at zero Li concentration to -1.20 in $LiCoO_2$. For each of the 44 structures, the charge around each of the oxygen ions was calculated by integrating the electron density within a sphere of radius r centered at the different oxygen sites. A constant sphere radius r was chosen for each structure and the oxygen charges in Fig. 6 are averages over all the oxygen ions of a given structure with a particular Li-vacancy arrangement. The radius r for each of the 44 structures was set equal to $\frac{1}{2}$ the equilibrium distance between nearest-neighbor oxygen ions of the close packed oxygen planes. For a representative subset of the 44 structures, we determined that these values for r are approximately equal to the radius that minimizes the quantity $\Delta q/\Delta V$ where Δq is the increase in the electron density and ΔV is the change in the sphere volume resuting from an incremental increase of the sphere radius. These values for r can, therefore, be regarded as an estimate of the oxygen radius within each structure. The values for r varied almost linearly with Li concentration between $r=1.21$ Å at $x=0$ to $r=1.25$ Å at $x=1$. The change in r with Li concentration is indicative of oxygen breathing observed in some ionic oxides.[18] It may be argued that the increase in integrated charge with Li concentration is a result of using a larger sphere radius at higher Li concentration. To determine whether or not this is the case, we calculated the charge density in structures with five different Li concentrations ($x=0$, $\frac{1}{4}$, $\frac{1}{2}$, $\frac{3}{4}$, and 1) in which the cell parameters and positions of the oxygen and Co ions were all kept identical. In this case, the effect of oxygen breathing is eliminated and we can use a fixed sphere radius r at all Li concentrations. Similarly to Fig. 6, the average oxygen charge varied linearly between -0.97 at $x=0$ to -1.25 at $x=1$. We emphasize that the oxygen charges in Fig. 6 are averages taken over all the oxygen ions within a given structure. Within some structures, the variation of the charge on the different oxygen ions is large, and this variation is a result of the local charge transfer of electrons from Li to its neighboring oxygen ions as illustrated in Fig. 5. The above results show that the charge on the oxygen ions is not fixed as the Li-vacancy configuration and/or Li concentration is changed. As will be discussed in Sec. IV, the increase of the average charge on the oxygen ions with Li concentration explains the variation of the c-lattice parameter in Li_xCoO_2 as a function of Li concentration.

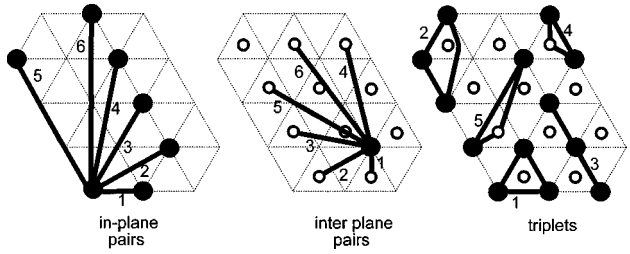

FIG. 7. Schematic illustration of the clusters used in the cluster expansions. The triangular lattice denotes the Li sites within a single Li plane, while the unfilled circles denote the projection of the Li sites of an adjacent Li plane. The points belonging to a particular cluster are connected by dark lines.

D. Cluster expansions and Monte Carlo simulations

To study phase stability at finite temperature, we need to construct a separate cluster expansion of the formation energy for each different host structure. Because of the large number of calculations involved in each cluster expansion, we did not construct a cluster expansion for the O1 host since, as described in Sec. III A, it is stable only at very dilute Li concentrations. In our calculations of the Li_xCoO_2 phase diagram O1 will therefore be treated as a line compound at $x=0$ and its free energy will be set equal to its energy.

A cluster expansion for the O3 host structure was constructed by applying an inversion method based on linear programming techniques[24] to the formation energies of 36 of the 44 different Li-vacancy configurations within the O3 host plotted in Fig. 3. The resulting cluster expansion contains 19 terms, including 12 pairs and 5 triplets. These clusters are illustrated in Fig. 7. The values of the ECI are plotted in Fig. 8(a) and are also listed in Table I. The ECI of Fig. 8(a) correspond to clusters that connect sites within the same Li plane and sites between adjacent Li planes. The root-mean-square (rms) difference between the 36 formation energy values used in the inversion method and the corresponding values as calculated with the cluster expansion is less than 5 meV. For the remaining eight Li-vacancy configurations not included in the inversion, the rms difference between their energies as calculated with the pseudopotential method and as predicted by the cluster expansion is 8 meV. This indicates that the cluster expansion for the O3 host has predictive capabilities. As can be seen from Fig. 8(a), the values of the ECI converge to zero as the number of sites or the separation between the sites in the cluster increases. The ECI corre-

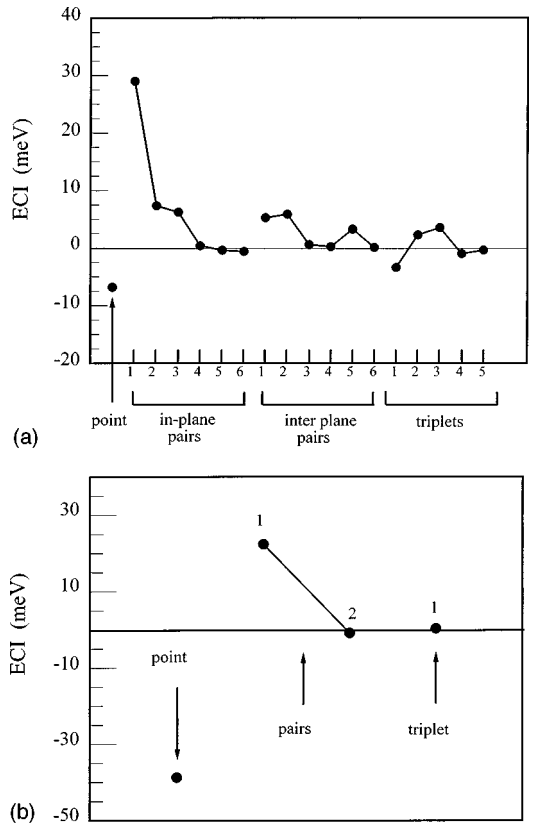

FIG. 8. Values of the ECI for (a) the O3 host and (b) the $H1$-3 host. Refer to Fig. 7 for an identification of the cluster corresponding to each effective cluster interaction.

sponding to the first-nearest neighbor in plane pair cluster is the largest, its value being at least three times larger than the other ECI.

As was pointed out in the previous section, the formation energy of the experimentally observed Li-vacancy ground-state ordering [Fig. 4(a)] at $x=\frac{1}{2}$ is practically degenerate with that of the configuration of Fig. 4(b). The cluster expansion plotted in Fig. 8(a) for the O3 host predicts that the ground-state configuration of Fig. 4(a) is more stable than the configuration of Fig. 4(b) by 5 meV. Although this difference is slightly larger than the difference calculated with the pseudopotential method, it is still smaller than the minimum numerical error expected from the pseudopotential method.

A second cluster expansion was constructed for the $H1$-3 host. This cluster expansion contains five terms. It was obtained by fitting the ECI to the formation energies of the five different Li-vacancy configurations within $H1$-3 plotted in Fig. 3. The ECI of this cluster expansion correspond to clusters within the same Li plane. Their values are illustrated in Fig. 8(b) and listed in Table II. Since occupied Li planes in the $H1$-3 host are further apart than in the O3 host, ECI corresponding to clusters connecting different Li planes have been neglected.

Both cluster expansions of the formation energy of the O3 and $H1$-3 hosts were implemented in Monte Carlo simulations in the grand canonical ensemble. To study the thermodynamics of Li and vacancy ordering in the O3 host, we used a Monte Carlo cell containing 3888 unit cells where each primitive unit cell corresponds to a $Li_x\varnothing_{1-x}CoO_2$ formula unit. For the $H1$-3 host, the Monte Carlo simulations were performed on a two-dimensional lattice, since the cluster expansion for this host only has ECI corresponding to clusters within the occupied Li planes. The Monte Carlo cell for the $H1$-3 host contained 900 primitive unit cells. At each temperature and chemical potential, 2000 Monte Carlo passes per lattice site were performed after which sampling oc-

TABLE I. ECI of the cluster expansion for the formation energies of the O3 host (second column) and of the cluster expansion for the c-lattice parameter for the O3 host (third column). Refer to Fig. 7 for an illustration of the clusters used in the cluster expansions.

Cluster type	V_α ECI (meV)	c_α ECI (Å)
Empty cluster V_0	−175.25	13.767
Point cluster	−6.83	0.175
In-plane pairs		
First	29.00	−0.078
Second	7.34	−0.034
Third	6.23	−0.054
Fourth	0.39	−0.016
Fifth	−0.41	−0.025
Sixth	−0.61	−0.008
Interplane pairs		
First	5.24	0.023
Second	5.84	−0.012
Third	0.57	−0.010
Fourth	0.22	−0.008
Fifth	3.26	−0.016
Sixth	0.10	0.002
Triplet clusters		
1	−3.38	0.067
2	2.27	0.004
3	3.53	−0.006
4	−1.00	0.002
5	−0.38	0.020

TABLE II. ECI of the cluster expansion for the formation energies of the H1-3 host (second column) and of the cluster expansion for the c-lattice parameter for the H1-3 host (third column). Refer to Fig. 7 for an illustration of the clusters used in the cluster expansions.

Cluster type	V_α ECI (meV)	c_α ECI (Å)
Empty cluster (V_0)	−125.54	12.843
Point cluster	−38.75	0.248
In-plane pairs		
First	22.42	−0.091
Second	−0.89	−0.004
Triplet cluster		
1	0.28	0.040

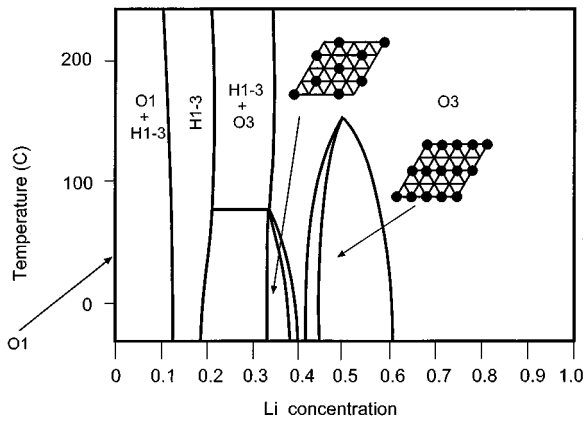

FIG. 9. The calculated Li_xCoO_2 phase diagram. The insets show the in-plane Li ordering predicted to be stable at $x=\frac{1}{2}$ and $\frac{1}{3}$.

curred over 4000 Monte Carlo passes. To investigate the relative stability between the O1 host, the O3 host, and the $H1$-3 host, we calculated the free energies of the latter two host structures as a function of Li concentration. These free energies were obtained by integrating the chemical potential obtained from the Monte Carlo simulations. The integration bounds were from zero Li concentration (where the free energy equals the ground-state energy) to the desired concentration x.

For both the O3 and the $H1$-3 host structures, we also cluster expanded the c-lattice parameters of the different Li-vacancy configurations whose geometries were optimized with the VASP pseudopotential code. A cluster expansion of the c-lattice parameter takes the form

$$c = c_0 + \sum_{\alpha} c_{\alpha}\varphi_{\alpha},$$

where c_0 and c_{α} are constant expansion coefficients and φ_{α} are polynomials in terms of occupation variables as described in Sec. II. For each Li-vacancy configuration, the equilibrium lattice parameters were converted to the hexagonal parameters of the O3 host. For both host structures, the cluster expansions of the c-lattice parameters contained the same clusters as used in the cluster expansion of the formation energies. The root-mean-square difference between the c-lattice parameters determined from the pseudopotential calculations and those as calculated with the resulting cluster expansion is 0.5% of the average c-lattice parameter of the O3 host. The values of the expansion coefficients c_0 and c_{α} for both the O3 and $H1$-3 hosts are listed in Tables I and II, respectively. These cluster expansions were used to determine the equilibrium lattice parameter as a function of Li concentration.

IV. PHASE DIAGRAM

The calculated equilibrium phase diagram of Li_xCoO_2 is presented in Fig. 9. It can be seen that the O3 host is predicted to be stable for Li concentrations above $x=0.3$. For Li concentrations above $x=0.6$, the Li ions and vacancies remain disordered within the O3 host even below room temperature. Figure 9 also indicates that when $x=0$ in Li_xCoO_2 the O1 host is the stable structure. At $x=\frac{1}{2}$, in agreement with the experimental observations of Reimers and Dahn,[3] we find that the Li ions order into rows alternated by rows of vacancies (see inset in Fig. 9). The order-disorder transition temperature of this phase is about 160 °C, which is 100 °C higher than the experimentally measured value.[3] This overprediction is typical of most first-principles phase diagram calculations within the local-density approximation. The stacking sequence of the in-plane-ordered Li arrangement of this phase is illustrated in Fig. 4(a). At $x=\frac{1}{3}$, the Li ions order in an arrangement in which the Li ions are spaced as far apart as possible. This ordered arrangement is illustrated in the inset in Fig. 9. The order-disorder transition temperature of this phase is about 80 °C. This ordered phase is not observed experimentally. However, in view of the expected overestimation of the order-disorder transition temperature in the local-density approximation, the true transition temperature is likely around or below room temperature. This may explain why it has not been observed experimentally.

For Li concentrations within a concentration interval of 0.05–0.10 centered at $x=0.15$, we find that the $H1$-3 host is more stable than both O1 and O3. In-plane Li ordering is predicted in the occupied Li planes of the $H1$-3 host at $x=\frac{1}{6}$. The in-plane ordered arrangement is the same as the in-plane ordered arrangement predicted at $x=\frac{1}{3}$ within the O3 host and illustrated in the inset of Fig. 9. The ordered Li arrangement within the $H1$-3 host is calculated to disorder at 130 °C through a second-order phase transition. It may be argued that the cluster expansion for the $H1$-3 host cannot be considered to be very accurate as it contains a relatively small number of ECI (i.e., five terms in the cluster expansion) and was constructed using a small amount of structures (i.e., formation energy values corresponding to five different Li-vacancy arrangements within the $H1$-3 host). To assess the accuracy, on the one hand, of the predicted stability range of $H1$-3 and, on the other, of the order-disorder transition temperature within $H1$-3, we investigated how small perturbations (not larger than 10 meV per formula unit) to the energies of the five structures used in the construction of the ECI for $H1$-3 affect these two properties. We found that, while the stability range of $H1$-3 with respect to O3 and O1 only changes negligibly, the order-disorder transition temperature does change much (of the order of 150 °C). Due to the uncertainty of the temperature at which the in-plane Li ordering at $x=\frac{1}{6}$ disorders within the $H1$-3 host, we have omitted it from the phase diagram of Fig. 9.

Experimentally, Ohzuku and Ueda[6] and Amatucci, Tarascon, and Klein[7] observed that during deintercalation, the O3 host undergoes a transformation to a new phase below $x=0.21$ that is stable as a single phase at $x=0.148$, but they did not identify this phase. The predicted stability of the $H1$-3 host around $x=0.15$ is consistent with this experimental finding. We compared calculated x-ray powder-diffraction patterns of the $H1$-3 phase with those observed experimentally[7] around $x=0.15$, and found that they agree well qualitatively. A detailed comparison of the calculated and experimental diffraction patterns at low Li concentrations has been published elsewhere.[29] In view of this agreement, we believe, therefore, that the experimentally observed phase transformation below $x=0.21$ is to the $H1$-3 host. This structure can be considered a stage-II compound.

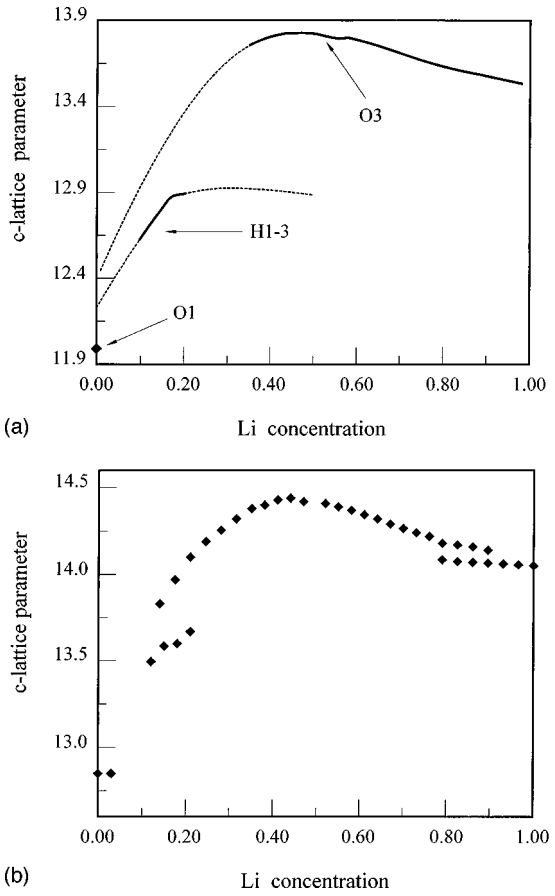

FIG. 10. Comparison between (a) calculated and (b) experimental (taken from Ref. 7) *c*-lattice parameter as a function of Li concentration (values are in Å). The calculated *c*-lattice parameters are also illustrated in the regions where the O3 and *H*1-3 hosts are metastable (dashed lines).

Figure 10 compares the calculated *c*-lattice parameters with that observed experimentally[7] as a function of Li concentration. The *c*-lattice parameters were calculated in the Monte Carlo simulations using the cluster expansions of the *c*-lattice parameters for the O3 and *H*1-3 hosts. Since the calculated order-disorder transition temperatures of the ordered phases at $x=\frac{1}{2}$ and $\frac{1}{3}$ within O3 are overpredicted, we calculated the *c*-lattice parameters at 130 °C (calculation temperature). This temperature is between the order-disorder transition temperatures of the $x=\frac{1}{2}$ phase and the $x=\frac{1}{3}$ phase and therefore properties calculated at this temperature will be most comparable with those measured experimentally at room temperature. We have plotted the *c*-lattice parameters of the O3 and *H*1-3 hosts over the range of Li concentrations for which these hosts can exist. This implies that the *c*-lattice parameters are also plotted for Li concentrations at which these hosts are predicted to be metastable. This enables us to more clearly identify trends.

The calculated *c*-lattice parameter of the O3 host is systematically predicted to be smaller than the experimentally observed value by approximately 4%. This is a direct result of the local-density approximation that is known to underpredict equilibrium lattice parameters. Despite the systematic underprediction, the qualitative agreement between the calculated and measured *c*-lattice parameter is remarkable. As Li is removed from the O3 host, the *c*-lattice parameter initially increases going through a maximum slightly below $x=0.5$ and then decreases as the Li concentration is lowered further.

V. DISCUSSION

Many features of the calculated phase diagram in Fig. 8 agree with experiment. Our first-principles calculations and previous ones[27] predict O1 to be more stable than O3 at zero Li concentration. The first-principles results described in Sec. III B, and the cluster expansion derived from these first-principle results, result in Li ordering at $x=\frac{1}{2}$ within the O3 host. Furthermore, we have been able to identify a new phase at $x=0.15$, of which the calculated diffraction patterns[29] agree qualitatively with the experimental patterns at that concentration.[7] Even the evolution of structural features such as the *c*-lattice parameter with Li concentration are qualitatively well reproduced (Fig. 10). Despite this agreement between calculated properties and experiment, there is one major disagreement at high Li concentration. As can be seen from Fig. 9, we do not find a two-phase coexistence region between $x=0.75$ and 0.93 as is observed experimentally.[3,6,7] This implies that this two-phase region is unlikely to be the result of an ordering reaction since we do not find any tendency for Li ordering above room temperature for $x>0.6$. We argue that the lack of agreement in this region of the phase diagram is a direct failure of the local-density approximation. While $LiCoO_2$ is an insulator,[4] substantial delithiation leads to metallic conductivity. We believe that this metal-to-insulator transition is responsible for the observed two-phase region. Recent experimental results by Tukamoto and West[43] provide evidence for the electronic nature of this transition. By substituting a dilute fraction of the Co^{3+} ions of $LiCoO_2$ by Mg^{2+} ions they found that Mg doping makes $LiCoO_2$ metallic without inducing any structural changes of the host. In parallel with this, they found that in the Mg-doped samples, the two-phase region is absent.

Experimentally, $LiCoO_2$ is observed to be a semiconductor in which the Co ions are in a low spin configuration.[4,5] Since the Co ions reside in an octahedral oxygen environment, the *d* levels of Co split into three t_{2g} bands and two e_g bands as a result of the ligand field produced by the negative oxygen ions. In an octahedral environment, the t_{2g} bands have a lower energy than the e_g bands. In low-spin $LiCoO_2$, the t_{2g} bands are completely filled with the six valence electrons of Co (i.e., Co^{3+}), while the e_g bands are empty. The experimentally measured gap between the t_{2g} and e_g bands is 2.7 eV.[4] First-principles calculations in the independent electron approach such as those performed in the local-density approximation,[13,44] qualitatively reproduce this electronic picture for $LiCoO_2$, although with a smaller band gap.

As Li is removed from $LiCoO_2$, an electron hole is created in the upper t_{2g} valence bands. When the Li concentration is below $x=0.75$ in Li_xCoO_2, there are presumably sufficient electron holes to allow for a high level of screening. At these Li concentrations, metallic behavior in which the electronic states are delocalized is therefore expected. This is indeed observed experimentally.[5] This picture is also qualitatively reproduced by our first-principles total-energy calculations, where we find that Li_xCoO_2 has partially filled va-

lence bands upon Li removal from $LiCoO_2$. For Li concentrations between $x=1$ and $x=0.75$, an insulator-to-metal transition must therefore exist. At very dilute electron-hole concentrations, the holes are likely to be unscreened or at least very poorly screened, causing them to remain localized. In this regime, electron correlations are important and first-principles investigations in the independent electron approximation, such as those performed in the local-density approximation, are likely to break down. To correctly study strongly correlated electronic systems it is necessary to resort to many-body theories that are currently intractable for systems with large unit cells. Our cluster expansion based on the local-density approximation is, therefore, not accurate to describe the thermodynamics for Li concentrations above the metal-insulator transition. This cluster expansion was constructed by fitting to formation energy values in which the holes in the t_{2g} bands are predicted to be delocalized. For concentrations well below the metal-insulator transition this is valid and accurate results can be expected. However, the cluster expansion will predict incorrect energetics for Li_xCoO_2 for Li concentrations above the metal-insulator transition since it will describe the system in this regime as if the electronic states are delocalized. Recent unrestricted Hartree-Fock calculations performed on Li-doped NiO have demonstrated that there can be a large energy gain when an electron hole goes form a delocalized state to a localized state.[45] This energy gain can be supplemented further by a local relaxation of the crystal in the vicinity of the localized hole.[45] Another effect for Li concentrations above the metal-insulator transition is the extra configurational entropy associated with the localized holes. The electronic contributions to the free energy are, therefore, very different depending on whether the holes are localized or delocalized and the differences are both of an energetic and entropic nature. Both entropic and energetic effects are expected to lower the free energy of insulating Li_xCoO_2. If this effect is strong enough to break the convexity of the free energy with Li concentration, a two-phase region between a metallic phase and a semiconducting phase will result.

It may be contended that the failure to predict the two-phase region between $x=0.75$ and 0.93 is not a failure of LDA, but results from the fact that the cluster expansion for the O3 host was not parametrized well in that region of composition. The structure with largest x (besides $LiCoO_2$) is at $Li_{0.833}CoO_2$. This concentration is in the middle of the experimentally observed two-phase region. Therefore, if phase separation is to be predicted between $x=0.75$ and 0.93, the energetics of structures at $x=0.833$ should indicate a tendency for phase separation. Nevertheless, as can be seen in Fig. 3, the formation energy of the structure at $x=0.833$ as predicted by LDA lies on the convex hull, a result which indicates a strong tendency for mixing.

Although the independent-electron approach in the local-density approximation seems to be inadequate for the study of Li_xCoO_2 for x in the vicinity of the metal-insulator transition, it is a powerful tool to help understand and predict the properties of Li_xCoO_2 away from the metal-insulator transition. For example, it is clearly capable in predicting the evolution of the c-lattice parameter as a function of Li concentration. An interesting feature about Li_xCoO_2 is that the c-lattice parameter (Fig. 10) of the O3 host is observed to go through a maximum at approximately $x=0.5$.[6,7] The cause for the initial increase in the c-lattice parameter as Li is removed from $LiCoO_2$ is intuitively clear. As Li is removed, the screening between the negatively charged oxygen planes is reduced resulting in an increased electrostatic repulsion between the oxygen ions facing each other across empty Li sites. Further removal of Li below $x=0.5$, however, results in a decrease in the c-lattice parameter. Since the screening effect of the positively charged Li ions is much lower at low Li concentrations, one would expect that the structure could not even keep its structural integrity because of the strong electrostatic repulsion between negatively charged oxygen ions. Nevertheless, both experimental observations and our calculations show that this does not take place, but surprisingly that the c-lattice parameter contracts. The reason for this can be attributed to a decrease in the average charge on the oxygen ions as the Li concentration is decreased. As shown in Fig. 6, the pseudopotential calculations predict that the average net charge on the oxygen ions decreases as the Li concentration is reduced. As a result, the electrostatic repulsion between the oxygen ions is lower at these concentrations. This effect in combination with the physical absence of Li ions that otherwise occupy a certain volume within the host structure results in the contraction of the host along the c axis at low Li concentrations.

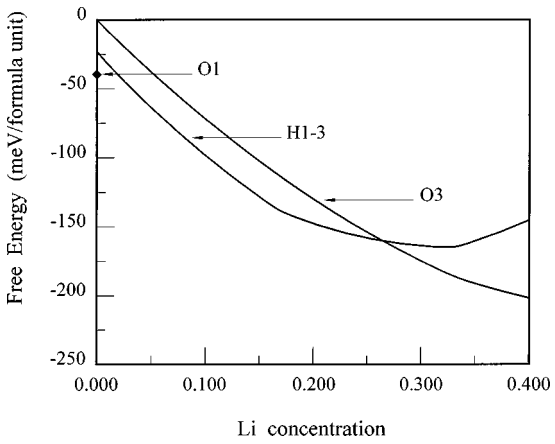

FIG. 11. The free energies at 30 °C of O3 and $H1$-3 as a function of Li concentration. Also illustrated is the energy of CoO_2 in the O1 host.

Another remarkable feature of Li_xCoO_2 is that the order-disorder transition temperature of the $x=\frac{1}{2}$ ordered phase is measured to be only slightly above room temperature, which is relatively low in comparison to other oxide systems. Although our calculations (see Fig. 9) based on the local-density approximation overpredicts this transition temperature by 100 °C the predicted transition temperature of 160 °C is still quite low. The origin of this result can be traced to the large electron transfer from Li to oxygen described in Sec. III C. As was indicated, the charge transfer from Li to the host is very local, and this local charge screens much of the positive charge on the Li ion thereby significantly reducing the effective interactions between Li^+ ions.

The occurrence of staging in layered intercalation compounds is not uncommon. It has been observed in transition-metal dichalcogenides[46,47] and is ubiquitous in graphite in-

tercalation compounds.[28] It is therefore not surprising that our first-principles calculations indicate that the $H1$-3 host, which can be considered a stage-II compound, is more stable than the O3 host at low Li concentration. In fact, as noted above, a comparison of the calculated x-ray powder-diffraction patterns of the $H1$-3 host with those measured experimentally[7] at low Li concentration is in good qualitative agreement.[29] The stability of the $H1$-3 host relative to the O3 host at low Li concentration can be understood by inspecting the free energies of $H1$-3 and O3 as a function of Li concentration at constant temperature. At dilute Li concentrations, the interaction between different Li ions is small. As a result, the free energy of both host structures depends primarily on the Li concentration with only a minor dependence on the interactions between Li ions. The free energies as a function of Li concentration of O3 and $H1$-3 are therefore more or less parallel at low Li concentration. This can be seen in Fig. 11, which illustrates the calculated free-energy curves of O3 and $H1$-3 as a function of Li concentration at room temperature. The $H1$-3 host, however, is more stable than O3 at $x=0$ as a result of the shuffle of the O-Co-O slabs adjacent to every other empty Li layer in $H1$-3. This relative stability persists for as long as the two free-energy curves are parallel. As the Li concentration increases, however, the Li planes of $H1$-3 saturate sooner than those of O3 since the former has only half the available Li planes. At these concentrations, the free energy of $H1$-3 becomes more sensitive to interactions between Li ions than that of O3. The free-energy curves are no longer parallel, and at one point the free energy of $H1$-3 crosses that of O3, making the latter phase more stable.

VI. CONCLUSION

In this work we have performed a first-principles investigation of the Li_xCoO_2 phase diagram. Our results indicate that first-principles investigations can give practical information and insights about the thermodynamic and phase stability properties of transition-metal oxide intercalation compounds. We find that at $x=\frac{1}{2}$, the Li ions order, in agreement with the observations of Reimers and Dahn.[3] We do not find the two-phase region observed experimentally at high Li concentration[3,6,7] and attribute this to the metal-insulator transition around that composition. At 15% Li concentration, we identify a stage-II compound to be stable.

ACKNOWLEDGMENTS

The authors would like to express their sincere gratitude to Dr. Adrian Kohan for helpful discussions on this work. This work was supported by the Department of Energy, Office of Basic Energy Sciences under Contract No. DE-FG02-96ER45571. We thank the San Diego Supercomputing Center for access to their C90 and the Center for Theoretical and Computational Materials Science of the National Institute of Sciences and Technology for generously providing us with computing resources. One of the authors (A.V.D.V.) gratefully acknowledges support from the DOE Computational Science Graduate Fellowship Program.

[1] K. Mizushima, P. C. Jones, P. J. Wiseman, and J. B. Goodenough, Mater. Res. Bull. **15**, 783 (1980).
[2] H. J. Orman and P. J. Wiseman, Acta Crystallogr., Sect. C: Cryst. Struct. Commun. **40**, 12 (1984).
[3] J. N. Reimers and J. R. Dahn, J. Electrochem. Soc. **139**, 2091 (1992).
[4] J. van Elp, J. L. Wieland, H. Eskes, P. Kuiper, G. A. Sawatzky, F. M. F. de Groot, and T. S. Turner, Phys. Rev. B **44**, 6090 (1991).
[5] J. Molenda, A. Stoklosa, and T. Bak, Solid State Ionics **36**, 53 (1989).
[6] T. Ohzuku and A. Ueda, J. Electrochem. Soc. **141**, 2972 (1994).
[7] G. G. Amatucci, J. M. Tarascon, and L. C. Klein, J. Electrochem. Soc. **143**, 1114 (1996).
[8] F. Ducastelle, *Order and Phase Stability in Alloys* (North-Holland, Amsterdam, 1991).
[9] D. de Fontaine, in *Solid State Physics*, edited by H. Ehrenreich and D. Turnbull (Academic, New York, 1994), p. 33.
[10] G. Ceder, Comput. Mater. Sci. **1**, 144 (1993).
[11] G. Ceder, in *Encyclopedia of Advanced Materials*, edited by D. Bloor, R. J. Brook, M. C. Flemings, and S. Mahajan (Pergamon, New York 1994), p. 1951.
[12] J. N. Reimers and J. R. Dahn, Phys. Rev. B **47**, 2995 (1993).
[13] M. K. Aydinol, A. F. Kohan, G. Ceder, K. Cho, and J. Joannopoulos, Phys. Rev. B **56**, 1354 (1997).
[14] G. Ceder, M. K. Aydinol, and A. F. Kohan, Comput. Mater. Sci. **8**, 161 (1997).
[15] M. K. Aydinol and G. Ceder, J. Electrochem. Soc. **144**, 3832 (1997).
[16] G. Ceder, A. F. Kohan, M. K. Aydinol, P. D. Tepesch, and A. Van der Ven, J. Am. Ceram. Soc. **81**, 517 (1998).
[17] G. Ceder and M. K. Aydinol, Solid State Ionics **109**, 151 (1998).
[18] P. D. Tepesch, A. F. Kohan, G. D. Garbulsky, G. Ceder, C. Coley, H. T. Stokes, L. L. Boyer, M. J. Mehl, B. Burton, K. Cho, and J. Joannopoulos, J. Am. Ceram. Soc. **79**, 2033 (1996).
[19] A. Zunger, in *Statics and Dynamics of Alloy Phase Transformations*, edited by P. E. A. Turchi and A. Gonis (Plenum, New York, 1994), p. 361.
[20] G. Ceder, M. Asta, W. C. Carter, M. Sluiter, M. E. Mann, M. Kraitchman, and D. de Fontaine, Phys. Rev. B **41**, 8698 (1990).
[21] M. Asta, R. McCormack, and D. de Fontaine, Phys. Rev. B **48**, 748 (1993).
[22] J. M. Sanchez, F. Ducastelle, and D. Gratias, Physica A **128**, 334 (1984).
[23] J. W. D. Connolly and A. R. Williams, Phys. Rev. B **27**, 5169 (1983).
[24] G. D. Garbulsky and G. Ceder, Phys. Rev. B **51**, 67 (1995).
[25] K. Binder and D. W. Heermann, *Monte Carlo Simulation in Statistical Physics* (Springer-Verlag, Berlin, 1988).
[26] C. Delmas, C. Fouassier, and P. Hagenmuller, Physica B&C **99**, 81 (1980).
[27] C. Wolverton and A. Zunger, Phys. Rev. B **57**, 2242 (1998).
[28] S. A. Safran, Solid State Phys. **40**, 183 (1987).
[29] A. Van der Ven, M. K. Aydinol, and G. Ceder, J. Electrochem. Soc. **145**, 2149 (1998).
[30] J. B. Goodenough, D. G. Wickham, and W. J. Croft, J. Phys. Chem. Solids **5**, 107 (1958).

[31] M. K. Aydinol and G. Ceder (unpublished).
[32] G. Kresse and J. Furthmuller, Phys. Rev. B **54**, 11 169 (1996).
[33] G. Kresse and J. Furthmuller, Comput. Mater. Sci. **6**, 15 (1996).
[34] D. Vanderbilt, Phys. Rev. B **41**, 7892 (1990).
[35] G. Kresse and J. Hafner, J. Phys.: Condens. Matter **6**, 8245 (1994).
[36] D. M. Ceperley and B. J. Alder, Phys. Rev. Lett. **45**, 566 (1980).
[37] J. P. Perdew and A. Zunger, Phys. Rev. B **23**, 5048 (1981).
[38] H. J. Monkhorst and J. D. Pack, Phys. Rev. B **13**, 5188 (1976).
[39] M. Methfessel and A. T. Paxton, Phys. Rev. B **40**, 3616 (1989).
[40] P. E. Blöchl, O. Jepsen, and O. K. Andersen, Phys. Rev. B **49**, 16 223 (1994).
[41] S. G. Louie, S. Froyen, and M. L. Cohen, Phys. Rev. B **26**, 1738 (1982).
[42] P. Tepesch, Ph.D. thesis, Massachusetts Institute of Technology, 1996.
[43] H. Tukamoto and A. R. West, J. Electrochem. Soc. **44**, 3164 (1997).
[44] M. T. Czyzyk, R. Potze, and G. A. Sawatzky, Phys. Rev. B **46**, 3729 (1992).
[45] W. C. Mackrodt, N. M. Harrison, V. R. Saunders, N. L. Allan, and M. D. Towler, Chem. Phys. Lett. **250**, 66 (1996).
[46] D. C. Dahn and R. R. Haering, Solid State Commun. **44**, 29 (1981).
[47] J. R. Dahn and W. R. McKinnon, J. Phys. C **17**, 4231 (1984).